Biophysical Letter

Inherent Force-Dependent Properties of β-Cardiac Myosin Contribute to the Force-Velocity Relationship of Cardiac Muscle

Michael J. Greenberg,[1] Henry Shuman,[1] and E. Michael Ostap[1,*]
[1]Pennsylvania Muscle Institute and Department of Physiology, Perelman School of Medicine at the University of Pennsylvania, Philadelphia, Pennsylvania

ABSTRACT The heart adjusts its power output to meet specific physiological needs through the coordination of several mechanisms, including force-induced changes in contractility of the molecular motor, the β-cardiac myosin (βCM). Despite its importance in driving and regulating cardiac power output, the effect of force on the contractility of a single βCM has not been measured. Using single molecule optical-trapping techniques, we found that βCM has a two-step working stroke. Forces that resist the power stroke slow the myosin-driven contraction by slowing the rate of ADP release, which is the kinetic step that limits fiber shortening. The kinetic properties of βCM are affected by load, suggesting that the properties of myosin contribute to the force-velocity relationship in intact muscle and play an important role in the regulation of cardiac power output.

Received for publication 18 July 2014 and in final form 6 November 2014.

*Correspondence: ostap@mail.med.upenn.edu

The cardiac cycle is a tightly regulated process in which the heart generates power during systole and relaxes during diastole. Appropriate power must be generated to effectively pump blood against cardiac afterload. Dysfunction of this cycle has devastating consequences for affected individuals.

Cardiac power output is regulated by several feedback mechanisms (e.g., neuronal, hormonal, mechanical) that ultimately lead to changes in the force and power output of the molecular motor, β-cardiac myosin (βCM). In isolated cardiac fibers and cardiomyocytes, loading the muscle during systole slows contraction and alters power output. It is widely believed that this slowing is partially due to force-induced inhibition of myosin ATPase kinetics, similar to the Fenn Effect in skeletal muscle. However, this hypothesis has not been directly tested at the molecular level. Much of our contemporary view of how power is generated in cardiac muscle is due to in vivo and isolated muscle-fiber studies (1). Substantial progress has been made in understanding the actomyosin interactions required for power generation, but resolving the molecular effects of mechanical load on the ATPase properties of βCM in intact muscle has been challenging. Nevertheless, determining the biophysical parameters that define βCM contractility is key to understanding cardiac regulation and the etiology of several muscle diseases (1).

In vitro assays using isolated contractile proteins have been central to advancing our understanding of contractility, although most experiments have been conducted at low resisting loads that do not mimic working conditions. Elegant optical trapping experiments have imposed loads on small ensembles of murine α-cardiac myosin at subsaturating [ATP] (2), and these experiments suggest that force slows α-cardiac myosin kinetics. The kinetic properties of α-cardiac myosin are substantially different from βCM, the primary isoform in the adult human myocardium (3). Thus, experiments using βCM must be performed to determine the unitary force-dependent kinetic parameters of this key molecular motor. We used optical trapping to measure the working-stroke displacement and force dependence of actin-detachment kinetics of single porcine βCM molecules at saturating ATP concentrations. These experiments allow direct measurement of the force-velocity relationship for single βCM molecules and reveal the mechanism of how loads regulate βCM-driven power output.

Using the three-bead geometry (4) in which an actin filament is strung between two optically-trapped beads and then lowered over a bead that is sparsely coated with purified full-length porcine ventricular βCM, interactions between single βCM molecules and actin were recorded at 10 μM ATP (Fig. 1 *A*) (5,6). Ensemble averages of these interactions were constructed to determine the size and kinetics of the working stroke (7,8). βCM has an average displacement (6.8 ± 0.04 nm) that is similar to previously characterized muscle myosins (9,10). Similar to skeletal muscle myosin (10), ensemble averages clearly show that the βCM working stroke is composed of two substeps with average displacements of 4.7 ± 0.05 nm and 1.9 ± 0.05 nm (Fig. 1 *B*). A single exponential function was fit to the rising-phase of the time-forward ensemble averages,

Editor: James Sellers.

http://dx.doi.org/10.1016/j.bpj.2014.11.005

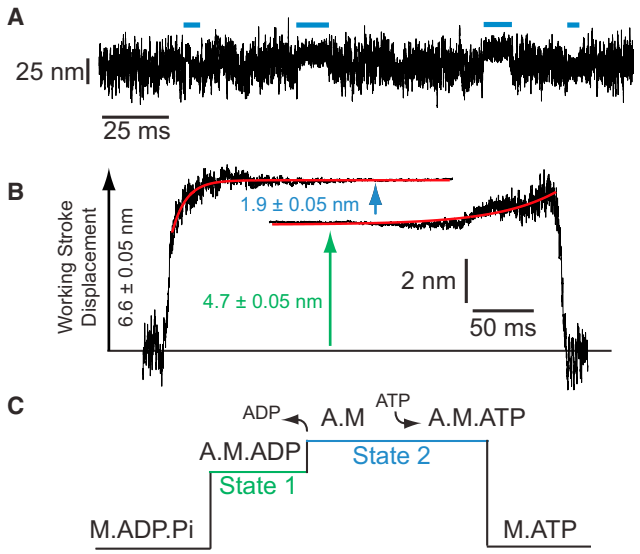

FIGURE 1 **(*A*) Representative data trace showing actomyosin displacements generated by βCM at 10 μM ATP. (*Blue lines*) Individual binding events. (*B*) Ensemble averages of the βCM working stroke generated from averaging 1295 binding interactions collected at 10 μM ATP. Single exponential functions were fit to the data (*red lines*) and the reported errors are the standard errors from the fit. (*C*) Cartoon showing an idealized actomyosin interaction with the corresponding mechanical and biochemical states. To see this figure in color, go online.**

yielding a rate (74 $\pm$ 2 s^{-1}) for the transition from state 1 to state 2 (Fig. 1 *C*). This rate is similar to the biochemical rate of ADP release measured for βCM (64 s^{-1}) (3), indicating that this structural transition is associated with the release of ADP. The rate of the rising phase of the time-reversed ensemble averages (22 $\pm$ 0.7 s^{-1}) reports the rate of exit from state 2 and is consistent with the biochemical rate of ATP binding and actomyosin detachment at 10 μM ATP (16 s^{-1}) (3) (Fig. 1 *C*).

To examine actomyosin detachment kinetics under working conditions, a positional feedback optical clamp was used to apply a dynamic load to the myosin, keeping the myosin at an isometric position during its working stroke (11). We measured the effect of force on the actin-attachment duration at 4 mM Mg.ATP to ensure that the rate of ATP binding is not rate-limiting for detachment. Increases in attachment durations are observed as the force on the myosin is increased (Fig. 2 *A*, *inset*). Assuming a two-state model (12), we expect the attachment durations to be exponentially distributed at each force with the force-dependent actin detachment rate, $k(F)$, given by (13)

$$k(F) = k_0 * e^{\frac{F \cdot d_{det}}{k_B * T}}, \quad (1)$$

where k_0 is the rate of the primary force-sensitive transition in the absence of force, F is the force on the myosin, d_{det} is the distance to the transition state (a measurement of force sensitivity), k_B is Boltzmann's constant, and T is the

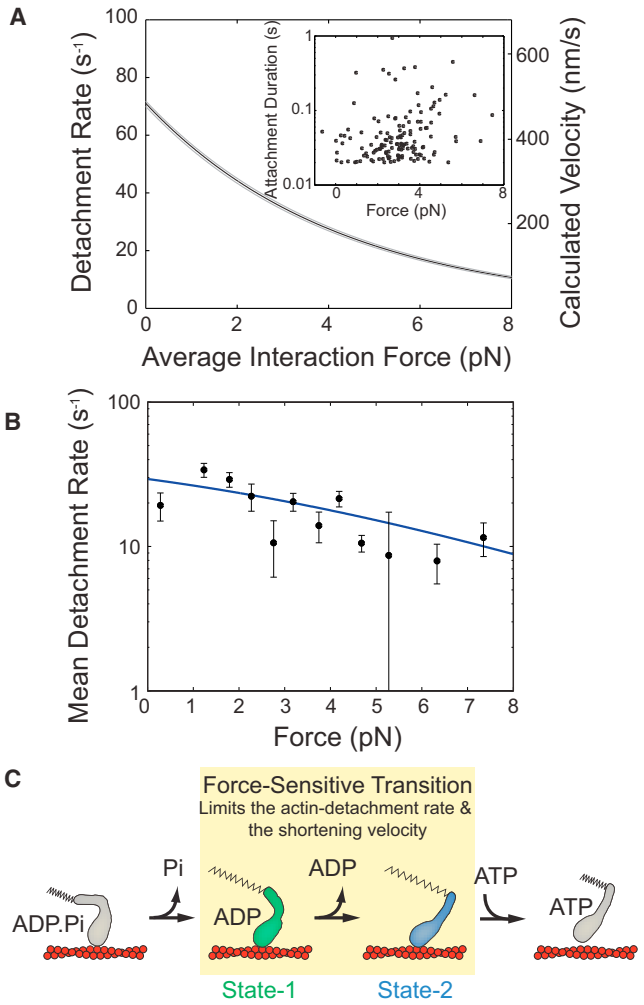

FIGURE 2 **(*A*, *Inset*) Single molecule actomyosin interactions were collected in the presence of the isometric optical clamp. The scatter plot shows 262 binding events. Attachment durations are exponentially distributed at each force. (*A*) The detachment rate as a function of force as determined by MLE fitting. (*Black line*) Best fit; (*small gray shaded area*) 95% confidence interval. (*Right axis*) Velocity, calculated by multiplying the displacement of the working stroke by the detachment rate. (*B*) The calculated mean detachment rate as a function of force. Attachment durations were binned according to the average force experienced by the myosin during the binding event. Error bars were calculated via bootstrapping simulations of each force bin. (*Blue line*) Expected mean detachment rate based on the MLE fitting and the limited temporal resolution of our experiment (see the Supporting Material for details). (*C*) Proposed model for how force slows shortening velocity. Force inhibits the mechanical transition associated with ADP release, slowing the rate of actomyosin detachment. To see this figure in color, go online.**

temperature. Maximum likelihood estimation (MLE) fitting Eq. 1 to the data yields a detachment rate (k_0 = 71 ($-1.0/+0.8$ s^{-1})) that is similar to the rate of ADP release measured for βCM (64 s^{-1}) (3) and the rate of the time-forward ensemble averages (74 $\pm$ 2 s^{-1}). Thus, the ADP

release step (and the accompanying state-1 to state-2 mechanical transition) is force-sensitive (d_{det} = 0.97 (−0.014/+0.011) nm). The value of d_{det} indicates that the ADP release step slows with increasing force, but less than some other characterized myosins (14). Using the values determined from the MLE fitting and the measured size of the working stroke, it is possible to calculate a force-velocity relationship for βCM, assuming the rate of ADP release limits actin motility (Fig. 2 *A*).

The MLE fitting of Eq. 1 assumes an exponential distribution of attachment durations at every force. As such, the MLE fitting of the raw data should yield correct values of the parameters k_0 and d_{det}, despite limitations of the temporal resolution of our experiment (see Supporting Material for detailed discussion of MLE fitting). Frequently, groups report the mean attachment duration as a function of force. However, the mean attachment duration at each force will be overestimated because some shorter binding events cannot be resolved. We provide a method for calculating the expected mean detachment rate based on the parameters determined from the MLE fitting, given the limited temporal resolution of the experiment, and verify the robustness of the MLE fitting (see the Supporting Material). For demonstration purposes only, Fig. 2 *B* shows that the measured mean detachment rate agrees well with the expected mean detachment rate based on the MLE fitting and the temporal resolution of the experiment. It should be emphasized that the relevant dissociation values are obtained from the MLE fitting in Fig. 2 *A* (see also Figs. S1–S3).

Our data demonstrate that at saturating [ATP], the detachment rate is limited by the ADP release step, which is the same transition that limits fiber shortening velocity (15). We propose that resisting loads slow ADP release and actin detachment by slowing the mechanical transition that accompanies ADP release (Fig. 2 *C*), thereby reducing the shortening velocity of muscle fibers. Thus, our data demonstrate that the intrinsic force-dependent properties of βCM contribute to the force-velocity relationship in the heart. It is important to note that our proposed mechanism does not rule out additional mechanisms by which force could directly modulate the activity of actomyosin such as force-induced reversal of the power stroke (11) or population of branched pathways (16,17).

Are the loads in our experiments physiologically relevant to contracting muscle? Modeling of the force per cross-bridge generated in isometric soleus muscle, which contains the βCM isoform, suggests a load of 2–4 pN per myosin (18). At these loads, we expect actin-detachment to slow up to threefold. Interestingly, βCM is substantially less force-sensitive than smooth muscle myosin (d_{det} = 2.7), suggesting that βCM can generate more power (the product of force and velocity) under load.

In conclusion, our data show that cardiac power output can be directly modulated by force at the level of single myosin molecules. These data will enable the comparison of how molecular changes, such as light-chain phosphorylation, pharmacological treatments, or mutations associated with cardiomyopathies, affect the ability of the myosin to generate power against the afterload.

SUPPORTING MATERIAL

Supporting Materials and Methods, one scheme, three equations, and three figures are available at http://www.biophysj.org/biophysj/supplemental/S0006-3495(14)01187-4.

This work was supported by the American Heart Association (grant No. 14SDG18850009 to M.J.G.) and National Institutes of Health (grant No. R01GM057247 to E.M.O. and grant No. K99HL123623 to M.J.G.).

SUPPORTING CITATIONS

References (19,20) appear in the Supporting Material.

REFERENCES and FOOTNOTES

1. Spudich, J. A. 2014. Hypertrophic and dilated cardiomyopathy: four decades of basic research on muscle lead to potential therapeutic approaches to these devastating genetic diseases. *Biophys. J.* 106:1236–1249.
2. Debold, E. P., J. P. Schmitt, …, D. M. Warshaw. 2007. Hypertrophic and dilated cardiomyopathy mutations differentially affect the molecular force generation of mouse α-cardiac myosin in the laser trap assay. *Am. J. Physiol. Heart Circ. Physiol.* 293:H284–H291.
3. Deacon, J. C., M. J. Bloemink, …, L. A. Leinwand. 2012. Identification of functional differences between recombinant human α and β cardiac myosin motors. *Cell. Mol. Life Sci.* 69:2261–2277.
4. Finer, J. T., R. M. Simmons, and J. A. Spudich. 1994. Single myosin molecule mechanics: piconewton forces and nanometre steps. *Nature.* 368:113–119.
5. Greenberg, M. J., T. Lin, …, E. M. Ostap. 2012. Myosin IC generates power over a range of loads via a new tension-sensing mechanism. *Proc. Natl. Acad. Sci. USA.* 109:E2433–E2440.
6. Laakso, J. M., J. H. Lewis, …, E. M. Ostap. 2008. Myosin I can act as a molecular force sensor. *Science.* 321:133–136.
7. Veigel, C., L. M. Coluccio, …, J. E. Molloy. 1999. The motor protein myosin-I produces its working stroke in two steps. *Nature.* 398: 530–533.
8. Chen, C., M. J. Greenberg, …, H. Shuman. 2012. Kinetic schemes for post-synchronized single molecule dynamics. *Biophys. J.* 102: L23–L25.
9. Tyska, M. J., E. Hayes, …, D. M. Warshaw. 2000. Single-molecule mechanics of R403Q cardiac myosin isolated from the mouse model of familial hypertrophic cardiomyopathy. *Circ. Res.* 86: 737–744.
10. Capitanio, M., M. Canepari, …, R. Bottinelli. 2006. Two independent mechanical events in the interaction cycle of skeletal muscle myosin with actin. *Proc. Natl. Acad. Sci. USA.* 103:87–92.
11. Takagi, Y., E. E. Homsher, …, H. Shuman. 2006. Force generation in single conventional actomyosin complexes under high dynamic load. *Biophys. J.* 90:1295–1307.
12. Huxley, A. F. 1957. Muscle structure and theories of contraction. *Prog. Biophys. Biophys. Chem.* 7:255–318.
13. Bell, G. I. 1978. Models for the specific adhesion of cells to cells. *Science.* 200:618–627.
14. Greenberg, M. J., and E. M. Ostap. 2013. Regulation and control of myosin-I by the motor and light chain-binding domains. *Trends Cell Biol.* 23:81–89.

15. Siemankowski, R. F., M. O. Wiseman, and H. D. White. 1985. ADP dissociation from actomyosin subfragment 1 is sufficiently slow to limit the unloaded shortening velocity in vertebrate muscle. *Proc. Natl. Acad. Sci. USA.* 82:658–662.

16. Linari, M., M. Caremani, and V. Lombardi. 2010. A kinetic model that explains the effect of inorganic phosphate on the mechanics and energetics of isometric contraction of fast skeletal muscle. *Proc. Biol. Sci.* 277:19–27.

17. Debold, E. P., S. Walcott, …, M. A. Turner. 2013. Direct observation of phosphate inhibiting the force-generating capacity of a miniensemble of myosin molecules. *Biophys. J.* 105:2374–2384.

18. Seebohm, B., F. Matinmehr, …, T. Kraft. 2009. Cardiomyopathy mutations reveal variable region of myosin converter as major element of cross-bridge compliance. *Biophys. J.* 97:806–824.

19. Kielley, W. W., and L. B. Bradley. 1956. The relationship between sulfhydryl groups and the activation of myosin adenosinetriphosphatase. *J. Biol. Chem.* 218:653–659.

20. Greenberg, M. J., K. Kazmierczak, …, J. R. Moore. 2010. Cardiomyopathy-linked myosin regulatory light chain mutations disrupt myosin strain-dependent biochemistry. *Proc. Natl. Acad. Sci. USA*. 107:17403–17408.

Inherent Force-Dependent Properties of β-Cardiac Myosin Contribute to the Force-Velocity Relationship of Cardiac Muscle

Michael J. Greenberg,[†] Henry Shuman,[†] and E. Michael Ostap[†]*
[†]Pennsylvania Muscle Institute and Department of Physiology, Perelman School of Medicine at the University of Pennsylvania, Philadelphia, PA, USA 19104-6083
*Correspondence: ostap@mail.med.upenn.edu

Supporting Materials

Detailed methods

Reagents, Proteins, and Buffers

Using the method of Kielley and Bradley (1), β-cardiac myosin was prepared from porcine ventricles that were cryoground in liquid nitrogen (Pel-freez Biologicals). Porcine βCM is 97% identical to human βCM whereas murine ventricular myosin is only 92% identical to human βCM. N-ethylmaldeimide modified myosin and actin were prepared from rabbit skeletal muscle as described (2). All actin was stabilized with a molar equivalent of rhodamine labeled phalloidin (Sigma). Unless otherwise mentioned, all experiments were conducted in KMg25 buffer (25 mM KCl, 1 mM DTT, 1 mM EDTA, 1 mM $MgCl_2$, 60 mM MOPS pH 7.0). ATP concentrations were determined spectrophotometrically before each experiment by absorbance at 259 nm, ε_{259} = 15,400 $M^{-1}cm^{-1}$.

Single Molecule Measurements

Myosin was spun down in an ultracentrifuge at 386000 x g for 30 minutes in the presence of 1 μM actin and 2 mM ATP to remove inactive protein (3). Motility chambers were prepared as previously described (2, 4). Solutions were added sequentially to the motility chambers as follows: 1 – 5 nM myosin in high salt buffer (KMg25 + 0.3 M KCl) (5 min); 1 mg/mL BSA in KMg25 (2x 5 min); 5 nM rhodamine-phalloidin decorated F-actin in KMg25 with 1 mg/mL glucose, magnesium ATP (either 10 μM for the measurement of the working stroke or 4 mM for the measurements of the force-dependent detachment rate), 1 mg/mL BSA, 192 U/ml glucose oxidase, and 48 μg/mL catalase (Sigma). Coated beads were then added to one side of the chamber to replace ~¼ the volume of the chamber. For the experiments measuring the size of the working stroke, bead-actin-bead dumbbells were constructed from 1 μm polystyrene beads coated with N-ethylmaleimide myosin (2). For the experiments conducted at saturating ATP concentrations, biotinylated actin and NeutrAvidin-coated beads were used as bead-actin-bead dumbbells due to the ATP-sensitivity of N-ethylmaleimide myosin. 25% biotinylated actin (Cytoskeleton Inc.) was added to the unlabeled actin to make biotinylated actin filaments and 1 μm polystyrene beads were incubated with NeutrAvidin overnight at room temperature. The chamber was sealed with silicon vacuum grease (Dow Corning).

Single molecule experiments were performed using the three-bead assay (5) as described previously (2, 4) in which an actin filament, strung between two optically-trapped beads, is brought in contact with a surface-attached bead that is sparsely coated with myosin. The trap stiffness for the measurement of the size of the working stroke was ~0.03 pN/nm. Data were collected at 20 kHz and then filtered to 10 kHz. Single molecule interactions at low ATP were selected using a covariance threshold as described previously (2) and interactions at high ATP were selected using a variance threshold to improve the time resolution. The beginning of the binding event is detected as the point in time in which the variance/covariance drops below a certain threshold and the end of the binding event is detected as the point in time in which the variance/covariance rises above this same threshold as described previously (2). The directionality of the actin was determined by visual inspection of the data and confirmed by ensemble averaging of individual data traces. Measurements of the force dependence of actin detachment were conducted using the isometric optical clamp to apply a load to the myosin (2, 6). For all of the experiments, data were collected from >6 different pedestals. The minimal temporal resolution for the data collected in the absence of the isometric optical clamp is 10 ms and 20 ms in the presence of the clamp.

In Vitro Motility Assays

Myosin was spun down at 386000 x g for 30 minutes in high salt buffer in the presence of 1 μM actin and 2 mM ATP to remove inactive protein (3). The concentration of protein was determined using a Bradford reaction. Myosin was diluted to 140 μg/mL and either 200 U/μL of calf intestinal alkaline phosphatase or an equivalent volume of buffer was added to the myosin. The myosin was incubated for 30 minutes at 37°C to dephosphorylate the regulatory light chains and then kept on ice for 30 minutes. Motility chambers were constructed as previously described (2). Solutions were added to the flow chamber as follows: 100 μg/mL myosin in high salt buffer (2 min); 1 mg/mL BSA in KMg25 (2x 1 min); 1 μM phalloidin stabilized actin in KMg25 (2 min); KMg25 + 5 mM ATP (2x); KMg25 (4x); 30 nM rhodamine phallodin stabilized actin in KMg25; activation buffer (KMg25 plus 192 U/ml glucose oxidase, 48 μg/mL catalase (Sigma), 1 mg/mL glucose, 5 mM ATP, and 0.5% methyl cellulose). Experiments were conducted at room temperature (20°C). Data were collected at 2 seconds per frame for 1 minute and 25 filaments were manually tracked. We found no significant effect of light-chain dephosphorylation on the unloaded sliding velocity of the myosin (0.55 ± 0.14 μm/s versus 0.53 ± 0.16 μm/s for untreated and treated myosin respectively; $p=0.56$).

Data and Statistical Analysis

Ensemble averages of the working stroke were constructed as previously described (2) and single exponential functions were fit to the data. To improve the signal-to-noise ratio, the traces from each bead were averaged before ensemble averaging. Reported errors are the standard errors of the fits to the data and are not a measurement of the variance in the population of events. It is important for us to note that the estimate of the error in the determined parameters is likely underestimated due to the extensions of the interactions, which is necessary for ensemble averaging.

For the experiments examining the force dependence of the actomyosin attachment durations, the relationship between the detachment rate and force, *k(F)* was modeled as a single-step process:

$$AM + ATP \xrightarrow{k(F)} A+M.ATP$$ Scheme 1

It is worth noting that the modeling does not depend on the nucleotide state of the myosin and therefore, this transition could just as easily start from a state binding ADP or ADP*Pi. The force dependence of the detachment rate was modeled using Equation 1. Given such a model, the distribution of attachment durations at a given force will be exponentially distributed. The model was fit to the data using maximum likelihood estimation (MLE) (2), permitting the measurement of both k_0 and d_{det}.

MLE analysis has been widely adopted in the single molecule field because it has several advantages over other fitting algorithms.

(1) Ordinary least squares fitting (a special case of the MLE), the most commonly used algorithm for fitting, assumes that all measurement errors are normally distributed. As such, it is very sensitive to outlying points. A more robust MLE fitting routine is less sensitive to outlying points. Moreover, least-squares fitting requires that (1) each measurement is independent and identically distributed and (2) the errors are normally distributed. In the case of single molecule data, there are often global constraints (e.g. the temporal resolution of the instrument) that cause a violation of these conditions and as such, standard fitting approaches are inaccurate and more robust fitting methods must be applied.

(2) Binning the data to generate histograms and then fitting distribution functions to those histograms causes information to be lost. The errors of the fit will depend on the size of the bins as well as the number of counts in each bin. As such, the measurement of error depends on the generation of the histograms themselves. MLE fitting does not require binning and therefore it does not suffer from this issue. Moreover, binning of force dependence data acquired here would cause deviations of the data from single exponential functions since each bin would include a range of forces, each with its own exponential rate constant (see Fig. S1).

(3) In our data, there are short-lived binding events that we are unable to resolve due to the temporal resolution of the experiment that lead to an underestimate of the mean detachment rate (a classical statistical parameter) (Fig. 2B). While it is true that the mean value of an exponentially decaying function is equal to the characteristic rate, the missing short-lived binding events will cause this rate to be underestimated. By using MLE fitting of the distribution to the data, it is possible to correct for this missing data.

95% confidence intervals for the MLE fitting were determined using bootstrapping simulations as we have done previously (2, 4). For each bootstrapped simulation, MLE fitting was used to determine the best-fit value (Fig. S2). The initial starting conditions for the fits were randomized using an annealing routine. 95% confidence intervals were calculated by determining the interval over which 95% of the simulated values were found.

<u>Simulation of the Force Dependence of Cardiac Myosin</u>

At high ATP concentrations there is a percentage of binding events that are below the temporal resolution of our instrument (20 ms). To test robustness of the MLE fitting routine where a percentage of the events are below the detection threshold, Monte Carlo simulations of the force-attachment duration relationship were generated in Matlab (Fig. S3). The forces measured in the feedback experiments are normally distributed to a first order approximation. A random number was drawn from a Gaussian distribution with a mean and standard deviation that matches the distribution of the experimental data set. Using this force and the values of d_{det} (0.97 nm) and k_0 (71 s^{-1}) determined from MLE fitting of the experimental data set, a random exponentially distributed number was selected from a distribution with a mean given by equation 1. This selection was repeated to generate a data set with 10000 points. From this data set, all events with a duration less than the temporal resolution of the experiment (20 ms) were removed. From the remaining simulated data set, 262 remaining binding events were selected to give a synthetic data set with the same size as the experimental data set. MLE fitting of this data set followed by 1000 rounds of bootstrapping simulations were carried out as described above to determine the best fit values and 95% confidence intervals.

Comparison of the Measured and Expected Mean Detachment Rates

MLE fitting of Equation 1 to the data assumes an exponential distribution of attachment durations at every force. When collecting the data at high ATP concentrations there are many binding events that are below the temporal resolution of our instrument. As such, the measured mean attachment duration will be greater than the true mean attachment duration calculated via MLE. As discussed above and demonstrated in Fig. S3, MLE fitting will provide the correct measurement of the parameters even when some events have durations below the temporal resolution of the instrument. To investigate how our measured mean attachment duration agrees with the expected mean attachment duration based on the parameters determined using MLE fitting and temporal resolution of the instrument, we note that the probability density function for the attachment duration as a function of force is given by:

$$PDF(F,t) = k(F) * e^{-k(F)*t} \qquad \text{(Equation S1)}$$

where t is the attachment duration and the force dependence of the detachment rate (i.e. k(F)) is given by equation 1. The expected mean value of the attachment duration measured at each force is given by:

$$< t >= \frac{\int_{t_o}^{t_f} t * PDF(F,t)\, dt}{\int_{t_o}^{t_f} PDF(F,t)\, dt} = \frac{\int_{t_o}^{t_f} t * k(F) * e^{-k(F)*t}\, dt}{\int_{t_o}^{t_f} k(F) * e^{-k(F)*t} dt} \qquad \text{(Equation S2)}$$

where t_o is the minimum observable event duration and t_f is the maximal event duration. Using the values for k_0 and d_{det} obtained from the MLE fitting, it is possible to calculate the expected mean attachment duration as a function of force, given the limited temporal resolution of the instrument. As can be seen (Figure 2B), the measured mean attachment rate (black dots) agrees well with the theoretical mean detachment rate based on the MLE fitting and the limited

temporal resolution of the instrument (blue curve). Error bars were determined by binning the data by force, generating 1000 bootstrap simulations of the data, and then calculating the standard deviation of these simulations. This was necessary due to the fact that points in each bin are exponentially, not normally distributed. It should be emphasized that the correct measurement is obtained from MLE fitting of the data and that this correction is not necessary to determine the values of k_0 and d_{det}.

Supporting Figure Legends

Figure S1: Cumulative dwell time distributions for data collected using the isometric optical clamp. Data were separated into low force (<2 pN, blue) or high force (>3 pN, red) events and cumulative dwell distributions were constructed. It should be noted that binning the data over a range of forces will result in an additional slow phase in the data due to force-induced slowing of the myosin kinetics over the wide range of forces included in each histogram. The cumulative dwell distribution (CDD) is given by:

$$CDD = y_0 - a * \exp(-k * x) \qquad \text{(Equation S3)}$$

where k is the rate of underlying process and y_0 and a are fitting parameters to correct for the fact that some events are below the detection threshold of the instrument. Fitting the distribution to the low force data, one obtains a rate of 58 ± 6 s^{-1}, similar to the rate over this force range obtained from MLE fitting of the full data set (Fig. 2). Fitting the distribution to the high force data, one obtains a rate of 34 ± 2 s^{-1}, similar to the rate over this force range obtained from MLE fitting of the full data set (Fig. 2). The high force data shows an additional slow component (<10% of the total amplitude) that is expected since binning the data over a wide range of forces will yield a range of force dependent rates. Taken together, the fitting shows that (1) the data are approximately exponentially distributed at each force, (2) forces that resist the working stroke slow the rate of actomyosin detachment, (3) the rates obtained with the MLE fitting of entire data set agree well with the rates measured from subsets of the data, and (4) despite missing some fast events, the data still allow for accurate determination of the rate constant that defines the primary force-sensitive transition.

Figure S2: Distribution of parameters determined from MLE fitting of the 1000 rounds of bootstrapping simulations. To determine the confidence intervals for the parameters d_{det} and k_0 determined via MLE fitting of the experimental data set, 1000 bootstrapped simulations of the data were generated. Bootstrapping of the data examines the sensitivity of the best-fit MLE parameters to outliers. For each simulation, MLE fitting of the data was used to determine the values d_{det} and k_0 from the simulated data. The starting values for each round of MLE fitting were randomized via several rounds of annealing to ensure that the results were not biased by the initial values. Shown are the histograms of the MLE best-fit values for (A) d_{det} and (B) k_0 for each simulation. The inset shows a magnification of the peak region. As can be seen, the values of d_{det} (0.97 nm) and k_0 (71 s^{-1}) determined from MLE fitting of the experimental data set agree well with the peaks of the histograms determined from the simulated data, showing that the MLE fit of the real data set is not biased by outlying points. Moreover, the values are tightly clustered around a single value without additional peaks, demonstrating that the values determined from MLE fitting of the experimental data are (1) not due to a local minima and (2) well defined by the data set.

Figure S3: Simulated data set showing the theoretical distribution of attachment durations. Using the values of d_{det} (0.97 nm) and k_0 (71 s^{-1}) determined from MLE fitting of the experimental data set and the minimum observable event duration (20 ms), a simulated data set with an equal number of points as the measured data set was generated. The experimental data set is colored red and the simulated data set is colored black. MLE fitting of the simulated data

set followed by 1000 rounds of bootstrapping yielded values of d_{det} (0.98 (-0.002/+0.001) nm) and k_0 (70 ± 0.11 s^{-1}) that agrees well with the input parameters to the simulation and the experimental data set. This demonstrates that MLE fitting is able to accurately determine values of d_{det} and k_0 with a simulated data set that has the same number of points and minimum observable event duration as the experimental data set.

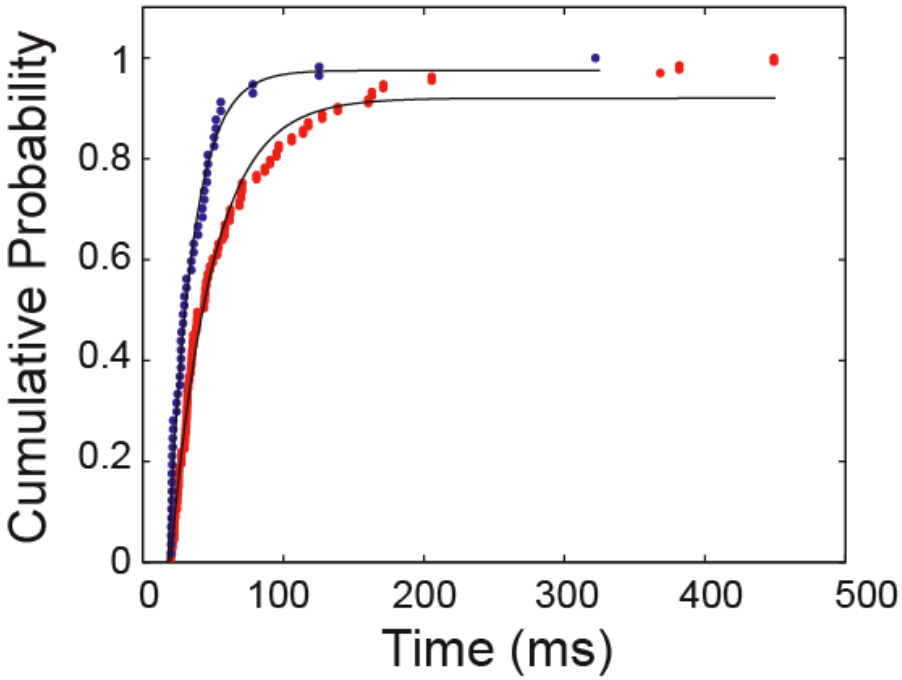
Cumulative Probability
1
0.8
0.6
0.4
0.2
0
0
100
200
300
400
500
Time (ms)

Figure S1

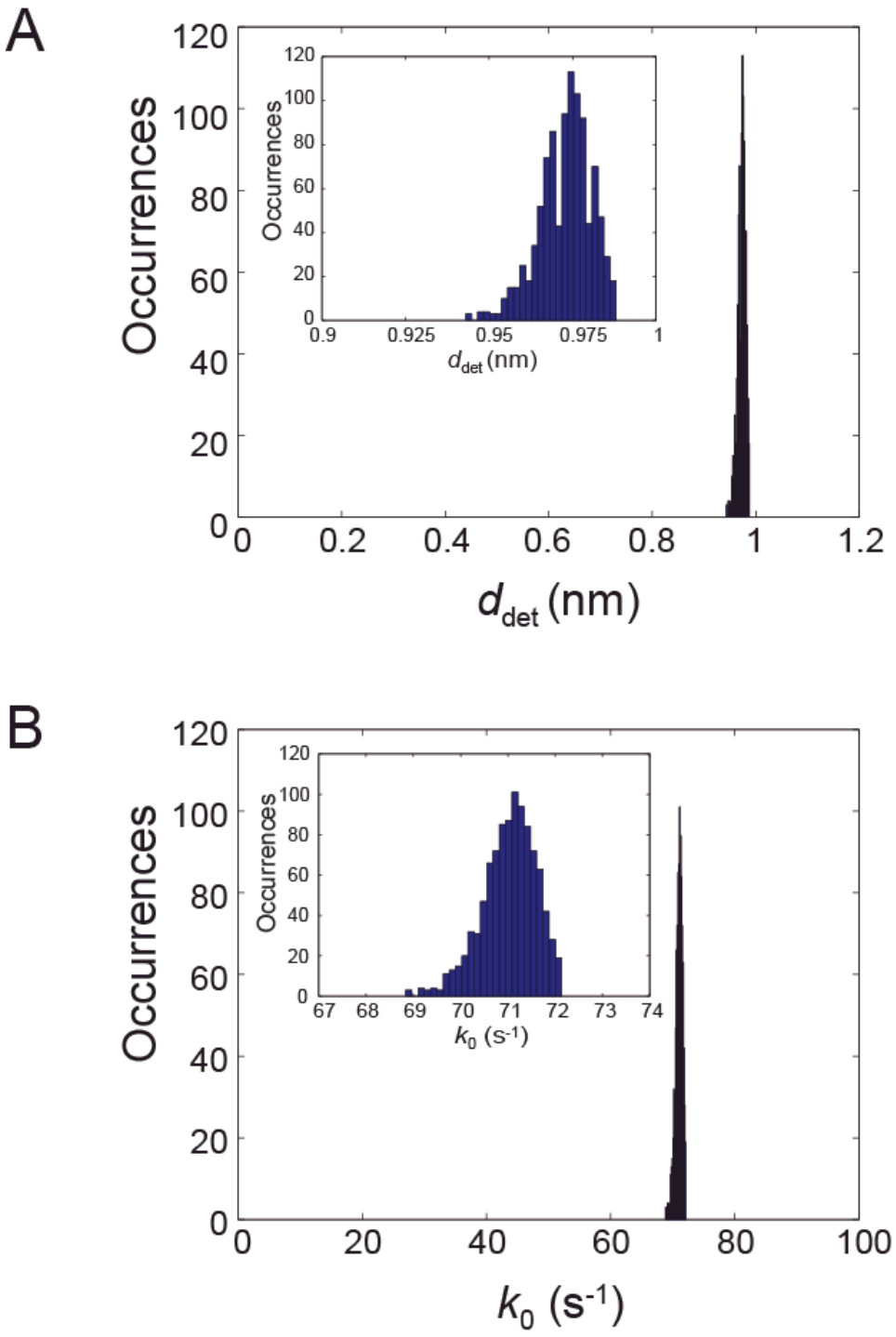

Figure S2

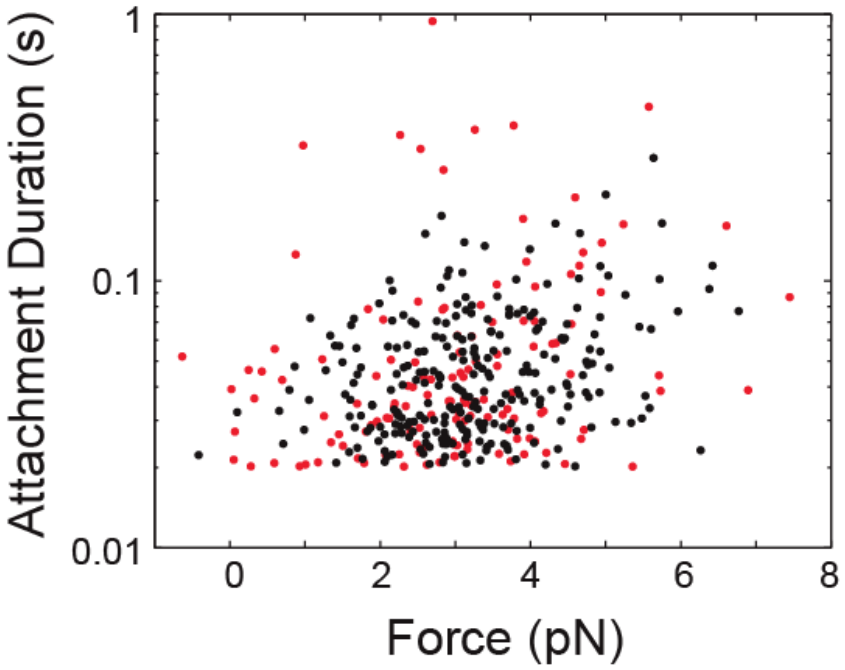

Figure S3

Supporting References

1. Kielley, W. W., and L. B. Bradley. 1956. The relationship between sulfhydryl groups and the activation of myosin adenosinetriphosphatase. The Journal of biological chemistry 218:653-659.
2. Laakso, J. M., J. H. Lewis, H. Shuman, and E. M. Ostap. 2008. Myosin I can act as a molecular force sensor. Science 321:133-136.
3. Greenberg, M. J., K. Kazmierczak, D. Szczesna-Cordary, and J. R. Moore. 2010. Cardiomyopathy-linked myosin regulatory light chain mutations disrupt myosin strain-dependent biochemistry. Proceedings of the National Academy of Sciences of the United States of America 107:17403-17408.
4. Greenberg, M. J., T. Lin, Y. E. Goldman, H. Shuman, and E. M. Ostap. 2012. Myosin IC generates power over a range of loads via a new tension-sensing mechanism. Proceedings of the National Academy of Sciences of the United States of America 109:E2433-2440.
5. Finer, J. T., R. M. Simmons, and J. A. Spudich. 1994. Single myosin molecule mechanics: piconewton forces and nanometre steps. Nature 368:113-119.
6. Takagi, Y., E. E. Homsher, Y. E. Goldman, and H. Shuman. 2006. Force generation in single conventional actomyosin complexes under high dynamic load. Biophysical journal 90:1295-1307.